Supporting Information for

Tuning the hydrogen evolution performance of 2D tungsten disulfide by interfacial engineering

Meiqin Shi,[a] Zhuangzhuang Jiang,[a] Bingbao Mei, [b] Yingying Li, [a] Fanfei Sun, [b] Haisheng Yu,[b*] and Yinghua Xu [a*]

[a] College of Chemical Engineering, Zhejiang University of Technology, State Key Laboratory Breeding Base of Green Chemistry-Synthesis Technology, Hangzhou 310032, Zhejiang, P. R. China

[b] Shanghai Synchrotron Radiation Facility, Shanghai Institute of Applied Physics, Chinese Academy of Science, Shanghai 201204, P. R. China

*Correspondence: xuyh@zjut.edu.cn (Y. Xu), yuhaisheng@sinap.ac.cn (H.Yu)

Experimental details

Table S1. Synthesis information for WO_3 and WS_2 samples

Precursor	Components	Programmed temperature method (Route Ⅰ~Ⅳ)	Samples
a	AMT	Ⅰ	WO_3-without
b	AMT+ NaCl	Ⅰ	WO_3
c	AMT+ H_2NCSNH_2	Ⅰ	WS_2-without
d	AMT+ H_2NCSNH_2+ NaCl	Ⅰ	WS_2, WS_2/NaCl
		Ⅱ	WC|WS_2-*T*
		Ⅲ	800-WC|WS_2-3
		Ⅳ	900-WC|WS_2-3

Ⅰ: heated up to 500 ℃ at rate of 10 ℃·min^{-1} and maintained 500 ℃ for 3 h with Ar flow (100 sccm);

Ⅱ: heated up to 500 ℃ at rate of 10 ℃·min^{-1} and maintained 500 ℃ for 3 h with Ar flow (100 sccm), then kept at 750 ℃ for 3 h (WC|WS_2-3), 6 h (WC|WS_2-6), 8 h (WC|WS_2-8), 10 h (WC|WS_2-10) and 16 h (WC|WS_2-16) with CO flow (100 sccm);

Ⅲ heated up to 500 ℃ at rate of 10 ℃·min^{-1} and maintained 500 ℃ for 3 h with Ar flow (100 sccm), then kept at 800 ℃ for 3 h (800-WC|WS_2-3) with CO flow (100 sccm);

Ⅳ heated up to 500 ℃ at rate of 10 ℃·min^{-1} and maintained 500 ℃ for 3 h with Ar flow (100 sccm), then kept 900 ℃ for 3 h (900-WC|WS_2-3) with CO flow (100 sccm).

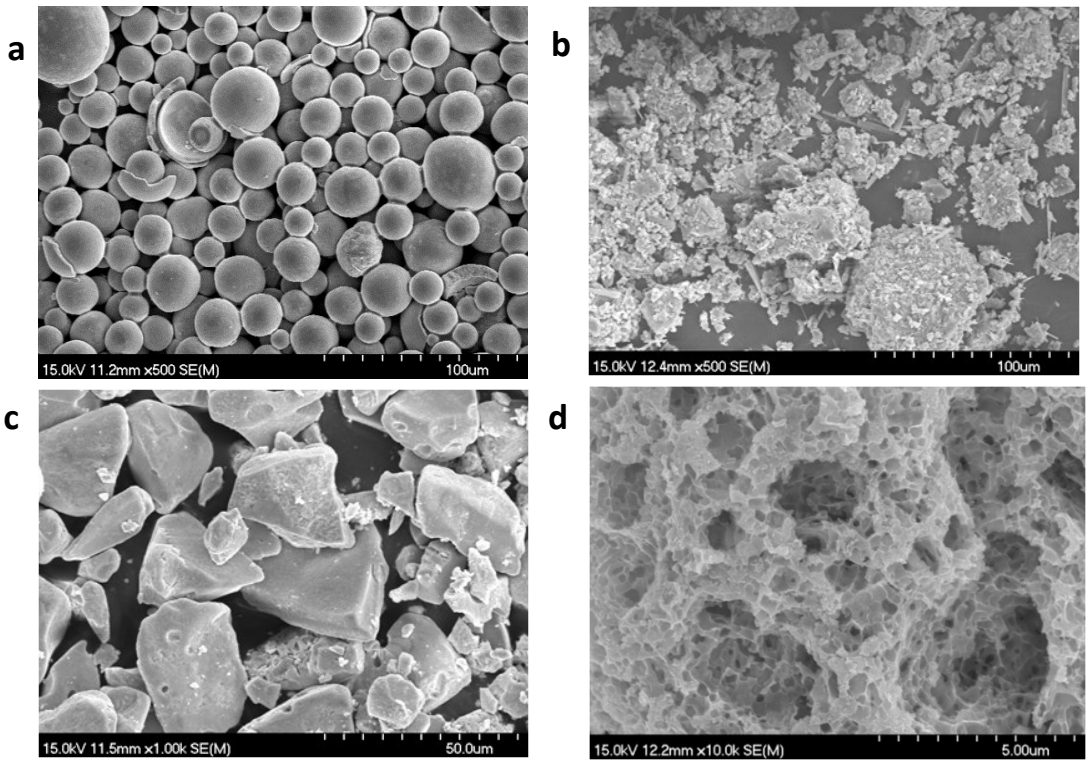

Figure S1.SEM images of (a) WO_3-Without, (b) WO_3, (c) WS_2-Without, (d) WS_2 composites.

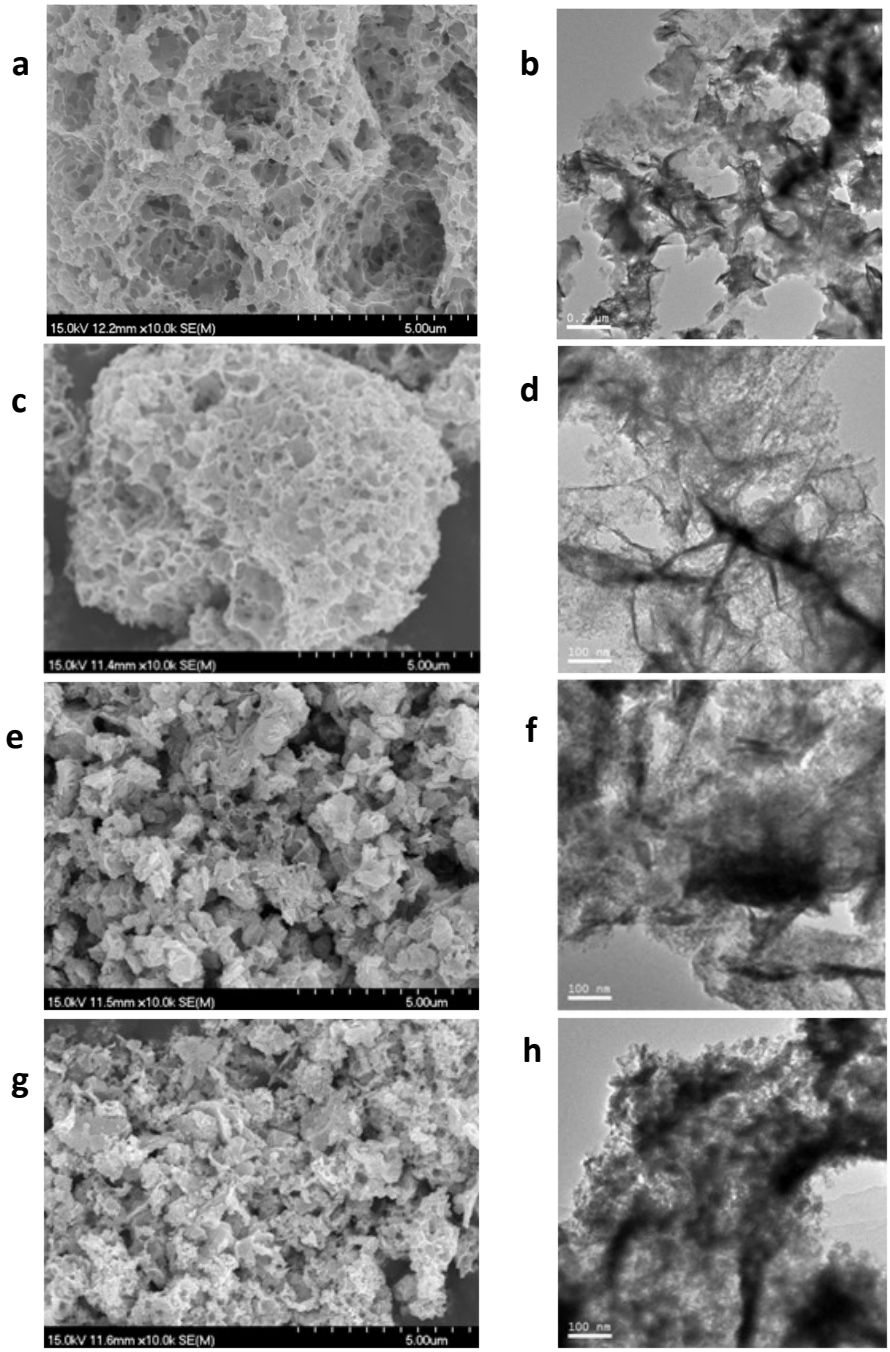

Figure S2. SEM and TEM images of WS_2 and WC|WS_2-3 under varied temperatures :(a) (b) WS_2, (c) (d) WC|WS_2-3, (e) (f) 800-WC|WS_2-3, (g) (h)900-WC|WS_2-3.

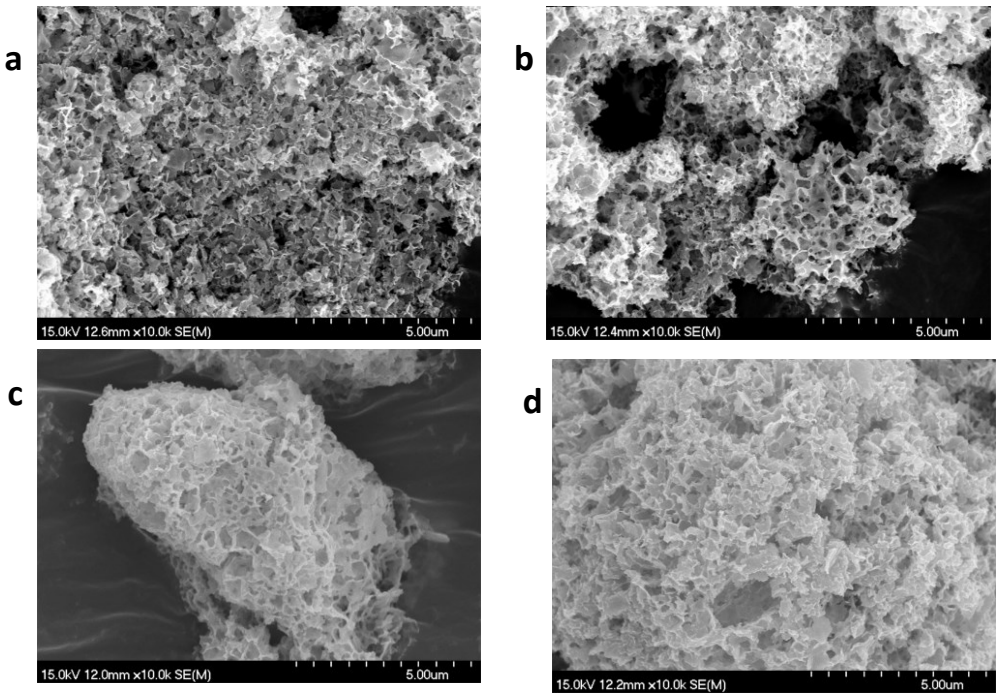

Figure S3. SEM images of WC|WS_2-T (6, 8, 10, 16 h):(a) WC|WS_2-6 sample, (b) WC|WS_2-8 sample, (c) WC|WS_2-10 sample, (d) WC|WS_2-16 sample.

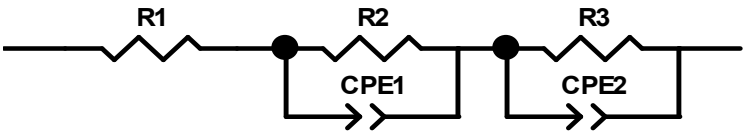

Figure S4. Electrical equivalent circuit model for fitting the EIS response of hydrogen evolution reaction on WS_2, WC|WS_2-10 and WC|WS_2-16 electrode.

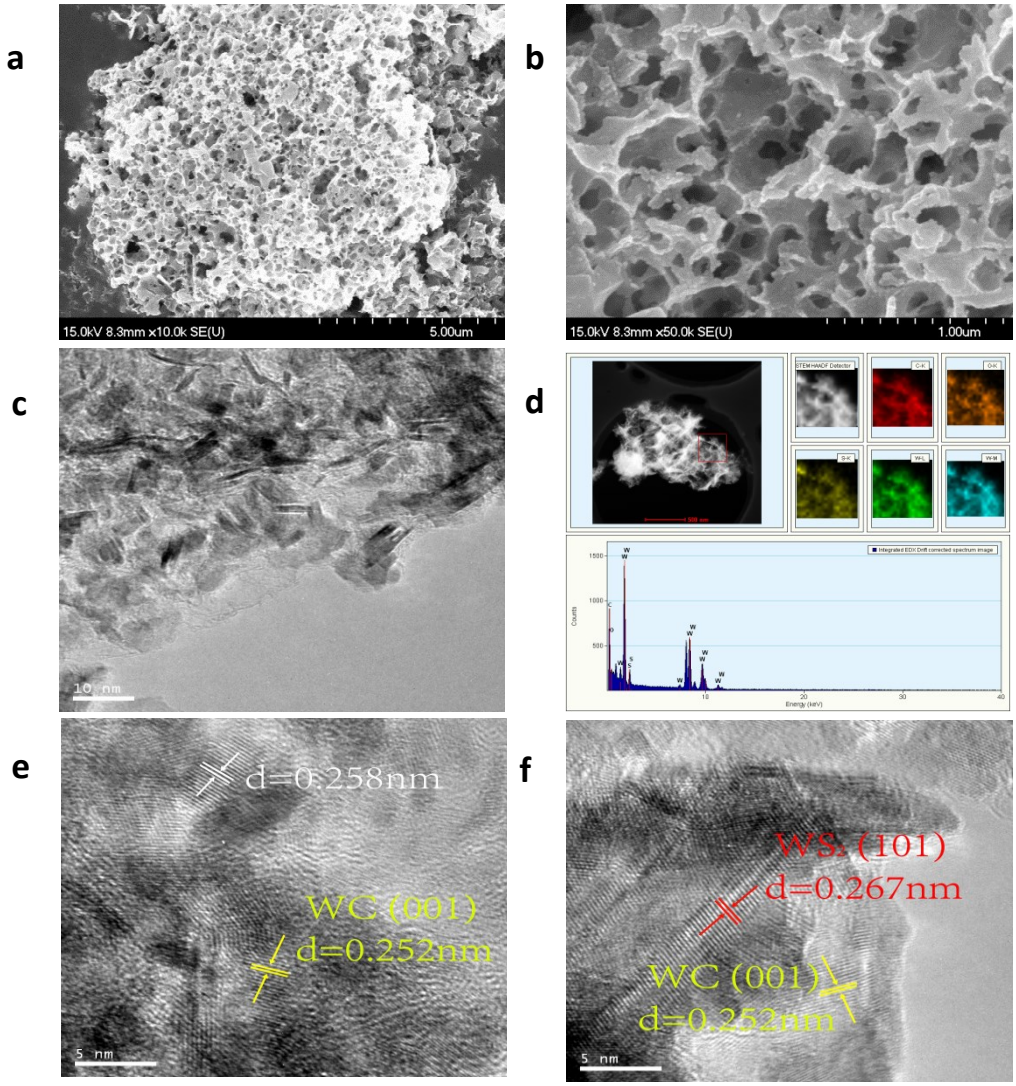

Figure S5. (a , b) SEM images ,(d) HRTEM image and the corresponding element mapping of C, S, W) , (c , e, f) TEM images of WC|WS_2-10 after long-term cycling in 0.5 M H_2SO_4.

As can be observed in Figure S5 (a, b), the catalyst WC|WS_2-10 still keeps the porous sponge-like morphology even after the long-term cycling in 0.5 M H_2SO_4, illustrating the morphology stability of catalyst. In the Figure S5 (e, f), lattice structures with interplanar spacings of 0.267 nm and 0.252 nm corresponding to the (101) planes of WS_2 and (100) planes of WC were found, and the fringe with spacing of 0.258 nm which can not be identified as WS_2 or WC were also observed, indicating that crystal structures remain the same after the cycling. Carbon layers on the edge or face of the nanosheets are clearly shown in Figure S5 (c), demonstrating the carbon structure would not be damaged in the HER process.

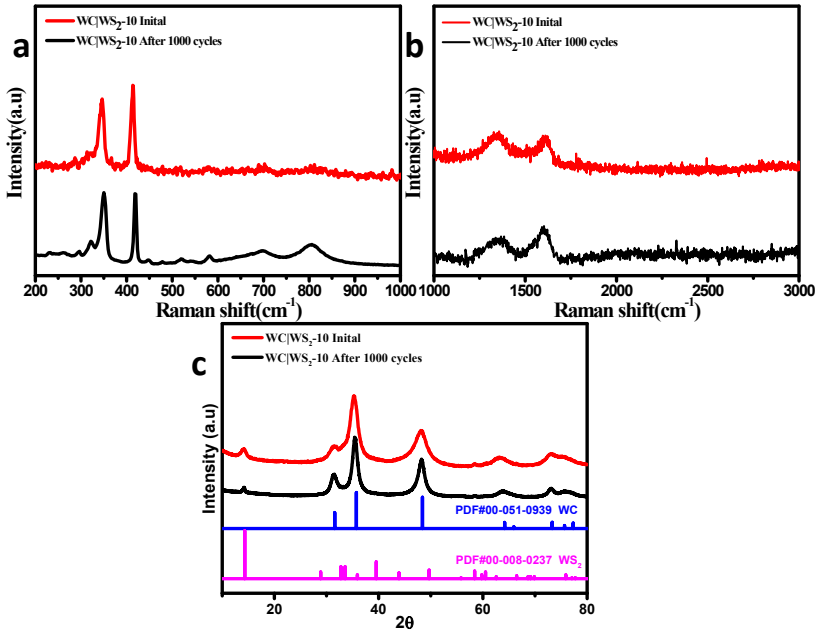

Figure S6. (a , b) The comparison of Raman spectra and (c) The XRD pattern of WC|WS_2-10 after continuous sweeps in 0.5 M H_2SO_4.

The comparison of Raman spectra and XRD pattern of WC|WS_2-10 before and after continuous sweeps in 0.5 M H_2SO_4 are displayed in Figure S6 (a, b). There is no visible difference can be observed in the XRD patterns, meaning the crystal structure is stable, which is consistent with the results of TEM. In the Raman spectra, the two characteristic peaks of E2g, A1g located at 355 and 412 cm^{-1} which attribute to in-plane and out-of-plane vibration modes of WS_2 still exist. The disorder-induced D and in-plane vibrational G peaks, located at ≈1350 cm^{-1} and ≈1580 cm^{-1} can also be confirmed, indicating the stability of crystal structure. It can be noticed that the bands at 708 and 806 cm^{-1} corresponding to the stretching modes of O-W-O bending become stronger after the long-term cycling, suggesting the surface oxygen group is increased due to the oxidation.

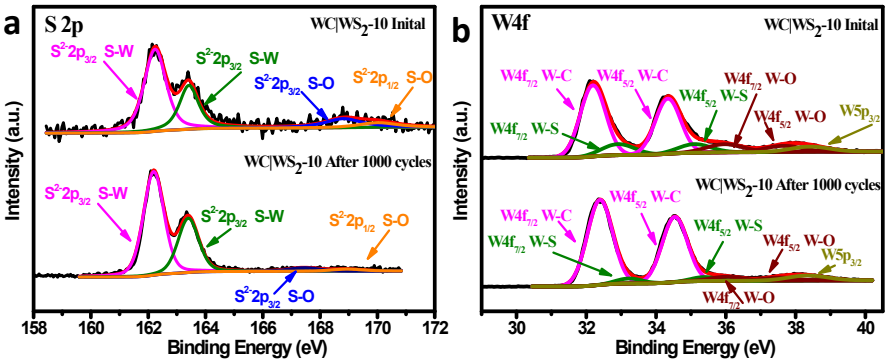

Figure S7. (a, b) The comparison of XPS spectrum of W 4f ,S 2p of WC|WS_2-10 after continuous sweeps in 0.5 M H_2SO_4.

The W 4f and S 2p XPS spectra of WC|WS_2-10 before and after continuous sweeps in 0.5 M H_2SO_4 was compared in Figure S7. As shown in Figure S7b, the W 4f XPS spectrum can be deconvoluted into three types of tungsten coordination for W–C, W–S and W–O. Comparing with the WC|WS_2-10 Initial composites , the binding energy of W-C peaks slightly shift from 32.19/ 34.34 eV to 32.39 / 34.54 eV, the binding energy of W-S peaks slightly shift from 32.90 / 35.10 eV to 33.2 / 35.38 eV, the binding energy of W-O peaks slightly shift from 35.97 / 37.65 eV to 36.02 / 37.53 eV in WC|WS_2-10 after 1000 cycles composites. There is no obvious change after the long-term cycling.

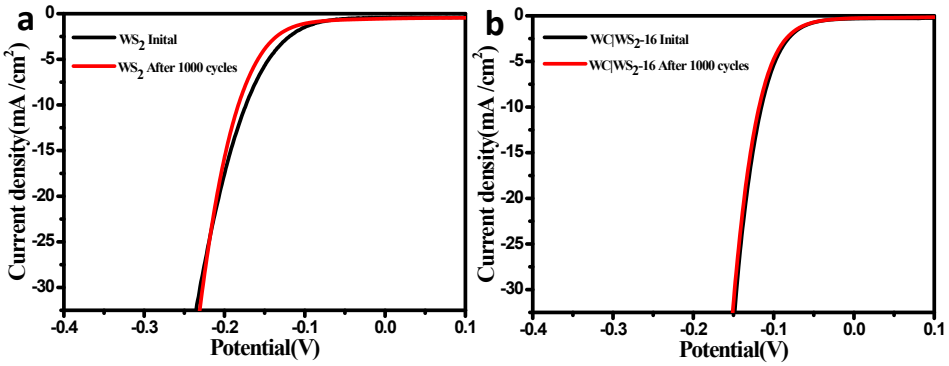

Figure S8. (a , b)The comparison of polarization curves of WS_2 and $WC|WS_2$-16 after continuous sweeps in 0.5 M H_2SO_4.

Figure S8 presents the comparison of polarization curves of WS_2 and $WC|WS_2$-16 after continuous sweeps in 0.5 M H_2SO_4. The declination is hardly found when the two CV curves recorded before and after 1000th CV cycles are compared which implies that WS_2 and $WC|WS_2$-16 are also stable electrocatalyst for the HER application.

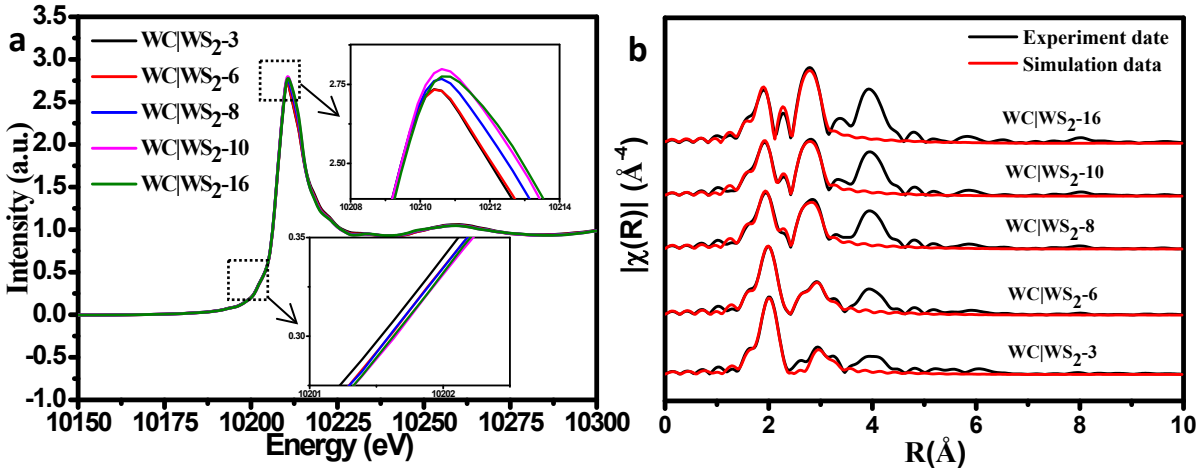

Figure S9. X-ray absorption near edge structure (XANES) spectra and fourier transforms (FT) K^2-weighted EXAFS spectra of varied materials.(a) XANES spectra of WC|WS_2-T (3, 6, 8, 10, 16 h),(b) The FT curves of WC|WS_2-T(3, 6, 8, 10, 16 h).

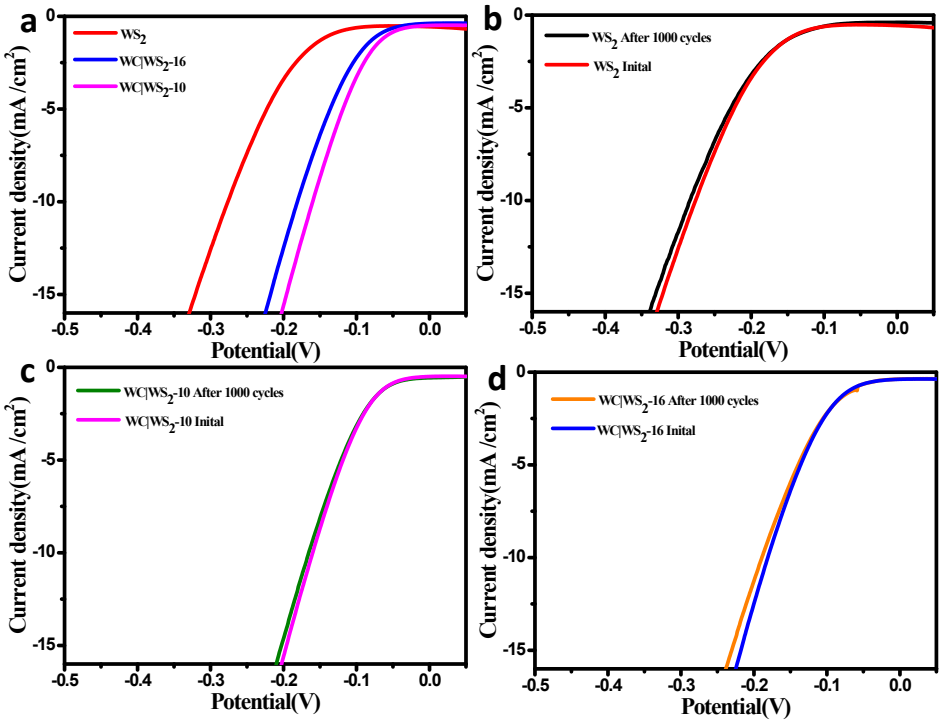

Figure S10. (a) Polarization curves of WS_2, WC|WS_2-10 and WC|WS_2-16 catalysts in 0.1 M KOH at a scan rate of 1 mv s^{-1}; (b, c, d) The comparison of polarization curves of WS_2, WC|WS_2-10, WC|WS_2-16 catalysts before and after continuous sweeps in 0.1 M KOH. All polarization curves are corrected for iR compensation.

HER performance of WS_2, WC|WS_2-10 and WC|WS_2-16 were examined by linear sweep voltammetry (LSV) in the region of -0.5-0.1 V with a scan rate of 1 mV s^{-1} in 0.1 M KOH. All the potentials were calibrated relative to an RHE according to the equation E (RHE) = E (Hg/HgO) + 0.059 × pH + 0.098 V. As shown in Figure S10 (a), the WC|WS_2-10 has the enhanced activity of 159 mV at a current density of 10 mA cm^{-2}, compared with those of WC|WS_2-16 (180 mV), and WS_2 (275 mV). However, we can notice the activity in alkaline solution of all these three samples is inferior to the corresponding one in acid solution. The durability of samples for HER in alkaline solution were also assessed by the constant CV in 0.1 M KOH, see in Figure S10 (b, c, d).The declination is hardly found when two CV curves recorded before and after 1000th CV cycles are compared which implies that the samples are stable for HER application in 0.1 M KOH.

Table S2. Comparison of different cheap and earth-abundant electrocatalysts available from literatures.

sample	specific surface area ($m^2 g^{-1}$)	an average pore size (nm)	Reference
WS_2/WO_2-6	50.2	3.3	[1]
MoS_2/WC/RGO	116 m	9.56	[2]
Porous WS_2	38	30~50	[3]
MoS_2-P	431.2	19	[4]

Table S3. Comparison of different cheap and earth-abundant electrocatalysts available from literatures.

Composition	Overpotential (mV) (at 10 mA cm^{-2})	Tafel Slope (mV/dec)	Stability	reference
WC|WS_2-3	-103	58	stable	This work
WS_2/WO_2-6 NRs	-147	63	stable	[1]
$W_{18}O_{49}$@WS_2 NRs	-310	86		[5]
MoS_2-P	– 251	80.5	stable	[4]
Metallic WS_2 nanosheets	-142	70	stable	[6]
WS_2/oCF	-250	99	stable	[7]
W_xC@WS_2	-146	61	stable	[8]
WC_x/C	-264	85	stable	[9]
N-WS_2	-197	69.69	stable	[10]
WS_2 nanosheets	-205	70	stable	[11]
1T-WS_2@SWCNT	-108	57	stable	[12]

References:

1. J. Wang, W. Wang, Z. Wang, J. G. Chen and C.-j. Liu, *ACS Catalysis*, 2016, **6**, 6585-6590.
2. Y. Yan, B. Xia, X. Qi, H. Wang, R. Xu, J. Y. Wang, H. Zhang and X. Wang, *Chem Commun (Camb)*, 2013, **49**, 4884-4886.
3. P. Gibot, J. Parmentier, L. Vidal, F. Schnell, H. Nouali and D. Spitzer, *Ceramics International*, 2017, **43**, 1443-1448.
4. X. Lu, Y. Lin, H. Dong, W. Dai, X. Chen, X. Qu and X. Zhang, *Scientific reports*, 2017, **7**, 42309.
5. B. Seo, H. Y. Jeong, S. Y. Hong, A. Zak and S. H. Joo, *Chemical communications*, 2015, **51**, 8334-8337.
6. M. A. Lukowski, A. S. Daniel, C. R. English, F. Meng, A. Forticaux, R. J. Hamers and S. Jin, *Energy & Environmental Science*, 2014, **7**, 2608.
7. X. Shang, K.-L. Yan, Z.-Z. Liu, S.-S. Lu, B. Dong, J.-Q. Chi, X. Li, Y.-R. Liu, Y.-M. Chai and C.-G. Liu, *Applied Surface Science*, 2017, **402**, 120-128.
8. F. Wang, P. He, Y. Li, T. A. Shifa, Y. Deng, K. Liu, Q. Wang, F. Wang, Y. Wen, Z. Wang, X. Zhan, L. Sun and J. He, *Advanced Functional Materials*, 2017, **27**, 1605802.
9. Z. Chen, M. Qin, P. Chen, B. Jia, Q. He and X. Qu, *International Journal of Hydrogen Energy*, 2016, **41**, 13005-13013.
10. C. Sun, J. Zhang, J. Ma, P. Liu, D. Gao, K. Tao and D. Xue, *J. Mater. Chem. A*, 2016, **4**, 11234-11238.
11. G.-Q. Han, Y.-R. Liu, W.-H. Hu, B. Dong, X. Li, Y.-M. Chai, Y.-Q. Liu and C.-G. Liu, *Materials Chemistry and Physics*, 2015, **167**, 271-277.
12. Q. He, W. Xu, S. Chen, D. Liu, M. Habib, Q. Liu, C. Wang, Y. A. Haleem, T. Xiang, C. Wu, A. Khalil, Q. Fang, Z. Niu and L. Song, *RSC Advances*, 2016, **6**, 87919-87925.